Computers and Chemical Engineering 192 (2025) 108893

Contents lists available at ScienceDirect

Computers and Chemical Engineering

journal homepage: www.elsevier.com/locate/cace

Two degrees of freedom control of a multistage power-to-methanol reactor

Tobias Keßler [a], Christoph Plate [b], Jessica Behrens [a], Carl J. Martensen [b], Johannes Leipold [a,*], Lothar Kaps [c], Andreas Seidel-Morgenstern [c], Sebastian Sager [b], Achim Kienle [a,d]

[a] Otto von Guericke University Magdeburg, Chair for Modeling/Automation, Universitätsplatz 1, Magdeburg, 39106, Germany
[b] Otto von Guericke University Magdeburg, Chair for Mathematical Algorithmic Optimization, Universitätsplatz 1, Magdeburg, 39106, Germany
[c] Max Planck Institute for Dynamics of Complex Technical Systems, PCF group, Sandtorstraße 2, Magdeburg, 39106, Germany
[d] Max Planck Institute for Dynamics of Complex Technical Systems, PSD group, Sandtorstraße 2, Magdeburg, 39106, Germany

ARTICLE INFO

Keywords:
Methanol synthesis
Power-to-methanol
Mathematical model
Artificial neural network
Dynamic optimization
Feedforward control
Feedback control

ABSTRACT

Power-to-methanol processes use green hydrogen, which is generated by electrolysis using regenerative energy, e.g. wind or solar energy. In this paper a novel control concept is proposed to handle fluctuations in the hydrogen feed due to unavoidable fluctuations in the energy supply. Focus is on a robust multistage reactor, with variable feed distribution as additional degrees of freedom. The controller uses dynamic optimization with a hybrid model for feedforward control of the feed distribution and simple PI control of the total carbon feed to compensate plant model mismatch and unforeseen disturbances. The hybrid model combines modeling from first principles with a neural network to capture the influence of catalyst dynamics on the reaction rates. The concept is validated with a simulation study using a detailed reference model.

1. Introduction

Methanol is an important starting material for many chemical processes. Traditionally, it is produced in large scale from fossil resources (natural gas and oil) and the resulting synthesis gas by hydrogenation of CO/CO_2 using a heterogeneous $Cu/ZnO/Al_2O_3$ catalyst under pressures in the range of 50-80 bar and temperatures of 200–250 degree Celsius (Asinger, 1986; Fiedler et al., 2000). Typically these processes are operated under steady state conditions with only minor fluctuations due to unforeseen disturbances.

Alternatively, power-to-methanol processes become more and more important (Schlögel, 2015; Burre et al., 2020; Mucci et al., 2023). Here, green hydrogen is obtained from water electrolysis with regenerative energy (e.g. solar or wind energy) and can react with CO/CO_2 from various sources like biogas (Vita et al., 2018; Theuerl et al., 2019), industrial exhaust gases (Nestler et al., 2018), or direct CO_2 air capture (Bos et al., 2020). Main objective of power-to-methanol processes is the reduction of greenhouse gas emission compared to traditional processes based on fossil feedstocks. However, utilization of regenerative energy sources for water electrolysis introduces unavoidable fluctuations in the hydrogen supply. To handle these fluctuations, different options are available, e.g. using intermediate storage (e.g. Mucci et al. (2023)), and/or robust reactor concepts, Fischer and Freund (2020) and Keßler and Kienle (2023) and/or suitable control concepts to compensate these fluctuations (e.g. Robinson and Luyben, 2011; Abrol and Hilton, 2012; Martin, 2016; Allman et al., 2019; Beek and Sadlowski, 2020). However, in most of these approaches linear models are applied and nonlinear reactor dynamics, which is a particular focus of this paper, are neglected.

This contribution is concerned with the multistage reactor which was introduced for methanol production in Keßler and Kienle (2023). The main idea in this concept is to handle fluctuations in the hydrogen feed supply by flexible distribution of the feed to the different stages of the reactor and thereby increase robustness. Since methanol synthesis is an exothermic reaction, flexible distribution of the feed to different reactors allows flexible heat management to avoid hot spot formation and achieve the desired conversion. For that purpose, in a first step a robust reactor design was proposed in Keßler and Kienle (2023) based on simultaneous steady state optimization of 50 characteristic disturbance scenarios. It was shown, that with this approach feasibility could be achieved under steady state conditions for given disturbance scenarios but not under transient dynamic conditions. Therefore, in a second step an open loop optimal control problem was solved by dynamic optimization to achieve feasibility for a given scenario also under transient conditions. The study was based on a detailed physical model of the methanol synthesis.

In the present paper, this strategy is extended in two directions. First, a hybrid mathematical model is used for nonlinear dynamic optimization. It is based on first principles using material and energy balances and comprises an artificial neural network for the prediction

* Corresponding author.
E-mail address: Johannes.leipold@ovgu.de (J. Leipold).

https://doi.org/10.1016/j.compchemeng.2024.108893
Received 30 May 2024; Received in revised form 18 September 2024; Accepted 9 October 2024
Available online 17 October 2024

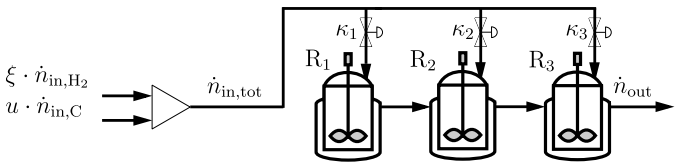

Fig. 1. Process flowsheet of the multistage reactor considered in this paper and in Keßler and Kienle (2023).

of the influence of the methanol catalyst dynamics on the reaction kinetics and thereby alleviates the modeling task. Second, to handle plant model mismatch and additional unforeseen disturbances, feedback control action is introduced with a simple PI controller, acting on the carbon feed supply to maintain constraints on conversion of the chemical reaction. The concept is evaluated step-by-step for a characteristic scenario taken from our previous work (Keßler and Kienle, 2023).

2. Mathematical models

2.1. Reactor model

In this paper a methanol reactor with three stages and a distributed feed as illustrated in Fig. 1 is considered.

The individual stages are modeled in this conceptual study in first approximation as well mixed diabatic CSTRs. Inside these reactors the heterogeneously catalyzed hydrogenation of a mixed CO and CO_2 feed is taking place according to

$$\mathrm{CO} + 2\,\mathrm{H_2} \rightleftharpoons \mathrm{CH_3OH}, \tag{1}$$

$$\mathrm{CO_2} + 3\,\mathrm{H_2} \rightleftharpoons \mathrm{CH_3OH} + \mathrm{H_2O}, \tag{2}$$

In addition, chemical conversion between CO and CO_2 following the water gas shift reaction plays an important role

$$\mathrm{CO} + \mathrm{H_2O} \rightleftharpoons \mathrm{CO_2} + \mathrm{H_2}\,. \tag{3}$$

The reactions are catalyzed by a standard $Cu/ZnO/Al_2O_3$ catalyst. The mathematical model of the individual stages assumes

- perfect mixing
- constant pressure
- thermodynamic equilibrium between the solid and the fluid phase

Under these assumptions the model equations of the individual stages follow from the quasihomogeneous material and energy balances. The component material balances read

$$\frac{\mathrm{d}}{\mathrm{d}t}\left(n_i^{\mathrm{G}} + n_i^{\mathrm{S}}\right) = \dot{n}_{\mathrm{in}} \cdot y_{i,\mathrm{in}} - \dot{n}_{\mathrm{out}} \cdot y_i + m_{\mathrm{cat}} \cdot \sum_j \nu_{i,j} \cdot r_j, \tag{4}$$

with

$$n_i^{\mathrm{G}} = n^{\mathrm{G}} \cdot y_i, \tag{5}$$

$$n^{\mathrm{G}} = \frac{\mathrm{p} \cdot \mathrm{V}}{\mathrm{R} \cdot T}, \quad \dot{n}_{\mathrm{out}} = \frac{\mathrm{p} \cdot \dot{V}_{\mathrm{out}}}{\mathrm{R} \cdot T}, \quad \dot{n}_{\mathrm{in}} = \frac{\mathrm{p} \cdot \dot{V}_{\mathrm{in}}}{\mathrm{R} \cdot T_{\mathrm{in}}}, \tag{6}$$

$$n_i^{\mathrm{S}} = \mathrm{m_{cat}} \cdot \mathrm{q_{sat}} \cdot \Theta_i, \tag{7}$$

Therein, Θ_i is the relative amount of all active sites of the catalyst surface occupied by component 'i'. It depends on the competitive adsorption equilibrium and is a function of the partial pressures of all components in the gas phase. A more detailed description is given in the reaction kinetics section and in Nikolić et al. (2022).

The total material balance follows from the component material balances by summation over all species 'i'. The total material balance is used to eliminate the molar flow rate of the outlet $\dot{n}_{\mathrm{out}}$ in Eq. (4). Together with Eqs. (5)–(7) the component material balances are obtained in final form as

$$\begin{aligned} &n^{\mathrm{G}} \cdot \frac{\mathrm{d}y_i}{\mathrm{d}t} + \mathrm{m_{cat}} \cdot \mathrm{q_{sat}} \cdot \mathrm{p} \cdot \left(\sum_k \frac{\partial \Theta_i}{\partial p_k} \cdot \frac{\mathrm{d}y_k}{\mathrm{d}t} - \sum_i \sum_k \left(\frac{\partial \Theta_i}{\partial p_k} \cdot \frac{\mathrm{d}y_k}{\mathrm{d}t} \right) \cdot y_i \right) = \\ &\dot{n}_{\mathrm{in}} \cdot \left(y_{i,\mathrm{in}} - y_i \right) + \mathrm{m_{cat}} \cdot \left(\sum_j \nu_{i,j} \cdot r_j - \sum_i \sum_j \left(\nu_{i,j} \cdot r_j \right) \cdot y_i \right). \end{aligned} \tag{8}$$

In a similar way the volumetric flow rate of the outlet is obtained from the total material balance according to

$$\begin{aligned} \dot{V}_{\mathrm{out}} &= \frac{\mathrm{V}}{T} \cdot \frac{\mathrm{d}T}{\mathrm{d}t} + \frac{T}{T_{\mathrm{in}}} \dot{V}_{\mathrm{in}} + \frac{\mathrm{m_{cat}} \cdot \mathrm{R} \cdot T}{\mathrm{p}} \\ &\times \left(\sum_i \sum_j \nu_{i,j} \cdot r_j - \mathrm{q_{sat}} \cdot \mathrm{p} \cdot \sum_i \sum_k \frac{\partial \Theta_i}{\partial p_k} \cdot \frac{\mathrm{d}y_k}{\mathrm{d}t} \right). \end{aligned} \tag{9}$$

To describe the temperature dynamics a quasihomogeneous energy balance is considered

$$\begin{aligned} &\frac{\mathrm{d}}{\mathrm{d}t} \left(\sum_i n_i^{\mathrm{G}} h_i^{\mathrm{G}} + \sum_i n_i^{\mathrm{S}} h_i^{\mathrm{S}} + m_{\mathrm{cat}} h_{\mathrm{cat}}^{*} \right) = \\ &\dot{n}_{\mathrm{in}} \sum_i \cdot y_{i,\mathrm{in}} h_{i,\mathrm{in}}^{\mathrm{G}} - \dot{n}_{\mathrm{out}} \sum_i \cdot y_i h_i^{\mathrm{G}} + \dot{Q}_{\mathrm{c}}, \end{aligned} \tag{10}$$

with enthalpies h and cooling rate $\dot{Q}_{\mathrm{c}}$. After differentiation and insertion of the above material balances the following differential equation for the reactor temperature is obtained

$$\begin{aligned} &\left(\underbrace{n^{\mathrm{G}} \cdot \bar{c}_{\mathrm{p}}^{\mathrm{G}}}_{\text{gaseous species}} + \underbrace{\mathrm{m_{cat}} \cdot q_{\mathrm{sat}} \cdot \bar{c}_{\mathrm{p}}^{\mathrm{S}}}_{\text{adsorbed species}} \overbrace{\rightarrow 0}^{} + \underbrace{\mathrm{m_{cat}} \cdot c_{\mathrm{p}}^{\mathrm{cat}}}_{\text{"dead" catalyst}} \right) \cdot \frac{\mathrm{d}T}{\mathrm{d}t} \\ &= \underbrace{-\dot{n}_{\mathrm{in}} \cdot \sum_i \int_{T_{\mathrm{in}}}^{T} c_{\mathrm{p},i}^{\mathrm{G}} \, \mathrm{d}T \cdot y_{i,\mathrm{in}}}_{\text{heat of transport}} \\ &\underbrace{- \mathrm{m_{cat}} \sum_j \Delta h_{\mathrm{R},j} \cdot r_j}_{\text{heat of reaction}} \underbrace{- \mathrm{K_W} \cdot \mathrm{A_W} \cdot \left(T - T_{\mathrm{c}} \right)}_{\text{heat of cooling}} \underbrace{- \sum_i \frac{\mathrm{d}n_i^{\mathrm{S}}}{\mathrm{d}t} \cdot \Delta \mathrm{h_{ads},}_i}_{\text{heat of adsorption}}, \end{aligned} \tag{11}$$

with

$$\bar{c}_{\mathrm{p}}^{\mathrm{G}} = \sum_i c_{\mathrm{p},i}^{\mathrm{G}} \cdot y_i, \quad \Delta \mathrm{h_{ads},}_i = h_i^{\mathrm{S}} - h_i^{\mathrm{G}}. \tag{12}$$

The heat capacity of the adsorbed phase is neglected as indicated on the left hand side of the above equation and the adsorption enthalpies are assumed to be constant. Caloric data can be found in Keßler and Kienle (2023).

For a detailed derivation of the quasihomogeneous model equations the reader is also referred to Keßler and Kienle (2023).

Reactor parameters used in this study are summarized in Table 1 for an industrial scale reactor according to Keßler and Kienle (2023).

Table 1
Reactor parameters.

Parameter	Value	Unit
V_{tot}	2.83	m^3
$m_{\mathrm{cat,tot}}$	2002	kg
ρ_{cat}	1770	kg m^{-3}
P	70	bar
K_W	250	W m^{-2} K^{-1}
A_W	18.85	m^2
q_{sat}	0.98	mol kg^{-1}
c_p^{cat}	1063	J kg^{-1} K^{-1}

2.2. Mechanistic model of the reaction kinetics

The mechanistic model of the reaction kinetics was taken from Seidel et al. (2018, 2020) with parameters from Seidel et al. (2021). The model used in the present paper represents the Langmuir Hinshelwood kinetics in Ref. Seidel et al. (2018) with lumped reactions steps for the reactions (1)–(3). It is based on a comprehensive set of experimental steady state and dynamic data provided in the PhD Thesis of Vollbrecht (2007). The experiments were performed in an isothermal isobaric well-mixed micro Berty reactor. The model assumes three different active centers on the surface of the considered $Cu/ZnO/Al_2O_3$ catalyst, namely, reduced centers (superscript 'red'), oxidized centers (superscript 'oxi') and active centers for heterolytic decomposition of hydrogen (superscript 'het'). The resulting expressions for the reaction rates are

$$r_{\mathrm{CO}} = (1-\phi)\cdot k_1 \cdot \left(p_{\mathrm{CO}} \cdot p_{\mathrm{H_2}}^2 - \frac{p_{\mathrm{CH_3OH}}}{K_1} \right) \cdot \Theta^{(\mathrm{oxi})} \cdot \Theta^{(\mathrm{het})^4}, \tag{13}$$

$$r_{\mathrm{CO_2}} = \phi^2 \cdot k_2 \cdot \left(p_{\mathrm{CO_2}} \cdot p_{\mathrm{H_2}} - \frac{p_{\mathrm{CH_3OH}} \cdot p_{\mathrm{H_2O}}}{K_2 \cdot p_{\mathrm{H_2}}} \right) \cdot \Theta^{(\mathrm{red})^2} \cdot \Theta^{(\mathrm{het})^4}, \tag{14}$$

$$r_{\mathrm{WGS}} = \frac{\phi}{1-\phi} \cdot k_3 \cdot \left(p_{\mathrm{CO_2}} - \frac{p_{\mathrm{CO}} \cdot p_{\mathrm{H_2O}}}{K_3 \cdot p_{\mathrm{H_2}}} \right) \cdot \Theta^{(\mathrm{red})} \cdot \Theta^{(\mathrm{oxi})}, \tag{15}$$

with equilibrium constants $\mathbf{K}$ according to

$$\log(\boldsymbol{K}) = \boldsymbol{\alpha_1} + \boldsymbol{\alpha_2}/T + \boldsymbol{\alpha_3} \cdot \log(T) + \boldsymbol{\alpha_4} \cdot T + \boldsymbol{\alpha_5} \cdot T^2, \tag{16}$$

and rate constants k_j.

$$k_j = \exp\left(\mathrm{A}_j - \mathrm{B}_j \cdot \left(\frac{\mathrm{T_{ref}}}{T} - 1 \right) \right). \tag{17}$$

Parameters $\boldsymbol{\alpha}_i$ in the above expression for the equilibrium constants have been taken from Skrzipek et al. (1994).

The relative amount of free oxidized surface centers $\Theta^{(\mathrm{oxi})}$, free reduced surface centers $\Theta^{(\mathrm{red})}$, and free surface centers for heterolytic hydrogen decomposition $\Theta^{(\mathrm{het})}$ follow from

$$\Theta^{(\mathrm{oxi})} = \left(1 + \boldsymbol{\beta}_{\mathrm{CO}}^{(\mathrm{oxi})} \cdot p_{\mathrm{CO}} \right)^{-1}, \tag{18}$$

$$\Theta^{(\mathrm{red})} = \left(1 + \boldsymbol{\beta}_{\mathrm{H_2}}^{(\mathrm{red})} \cdot p_{\mathrm{H_2}}^{0.5} \right)^{-1}, \tag{19}$$

$$\Theta^{(\mathrm{het})} = \left(1 + \boldsymbol{\beta}_{\mathrm{CO_2}}^{(\mathrm{het})} \cdot p_{\mathrm{CO_2}} \right)^{-1}. \tag{20}$$

It should be noted, that the above expressions are a reduced version of the full model in Seidel et al. (2018, 2020, 2021). Expressions corresponding to zero $\boldsymbol{\beta}$ parameters obtained from the parameter fit over a wide range of operating conditions in Seidel et al. (2021), i.e. pressures 30–60 bar, temperatures 500–530 K and various compositions, were neglected for simplicity. For refitting the model to other, entirely different data e.g. in terms of pressures, temperatures or catalyst, the original full model should be taken into account.

In contrast, to traditional kinetic models for methanol synthesis (Graaf et al., 1986, 1988; Bussche and Froment, 1996), dynamic changes of the oxidation state of the catalyst depending on the reducing and oxidizing potential of the gas phase is taken into account. This is described by the following differential equation

$$\frac{\mathrm{d}\phi}{\mathrm{d}t} = \mathrm{k}_1^+ \cdot \left(y_{\mathrm{CO}} \cdot \Delta\phi - K_1^{+-1} \cdot y_{\mathrm{CO_2}} \cdot \phi \right) + \mathrm{k}_2^+ \cdot \left(y_{\mathrm{H_2}} \cdot \Delta\phi - K_2^{+-1} \cdot y_{\mathrm{H_2O}} \cdot \phi \right), \tag{21}$$

where y_i are the mole fractions of the different components in the gas phase, $\Delta\phi = \phi_{max} - \phi$, and

$$\boldsymbol{K}^+ = \exp\left(\frac{-\boldsymbol{\Delta G}}{\mathrm{R} \cdot T} \right). \tag{22}$$

All parameters of the reaction kinetics used in this paper are given in the present nomenclature in Table 2.

Finally, it is important to note that the model is clearly nonlinear, mainly due to the exponential temperature dependence of the reaction rate constants according to Arrhenius.

2.3. Hybrid model of the reaction kinetics

The influence of the catalyst dynamics on the reaction rates in the above model was described by prefactors

$$\boldsymbol{\gamma} = \left[1-\phi, \phi^2, \frac{\phi}{1-\phi} \right]. \tag{23}$$

in the rate expressions (13)–(15). They were derived based on heuristic assumptions and empirical testing in Seidel et al. (2018, 2020). Accordingly, the reaction rate vector can be expressed as

$$\bar{r}_i = \gamma_i(\mathbf{x})\, r_i, \quad i \in \left(\mathrm{CO}, \mathrm{CO_2}, \mathrm{RWGS} \right) \tag{24}$$

A detailed derivation of the $\boldsymbol{\gamma}$ functions from extended experimental data and/or microkinetic models would be extremely challenging. Further it is assumed that such level of detail is not required for applications in process control to be considered in this paper. It has therefore been suggested (Martensen et al., 2023), to replace (23) with an artificial neural network (ANN) that is in the end directly trained with dynamic data. Such a hybrid model structure should combine good predictability due to the inclusion of physico-chemical a priori knowledge with reduced effort for model generation due to modeling the influence of partly unknown kinetics with a data driven approach. To test this hypothesis, the neural network is trained in a first step with data generated by the mechanistic model of a single CSTR under isothermal isobaric conditions. Thereby it is assumed that the ANN may depend not only on ϕ but all concentration variables. Later the resulting hybrid model is used for optimization and control of the nonisothermal multistage reactor in Fig. 1. The control strategy based on the hybrid model is then tested with the detailed mechanistic model.

The network is initially trained with a synthetic noise-containing data set, following the approach described in Martensen et al. (2023) and utilizing a likelihood objective of maximum a posteriori. Through Monte Carlo sampling, hyperparameter tuning has been conducted to determine a suitable architecture of the neural network comprising the choice of activation function as well as the number/quantity of hidden layers and their respective sizes. The data set is divided into separate training and testing sets. The most suitable architecture is chosen based on the Bayesian Information Criterion, leading to the selection of a neural network with one hidden layer and two neurons, employing the selu activation function. The output layer is equipped with the softplus activation function to enforce positive definite outputs. For the details concerning the determination of the network structure the reader is referred to Martensen et al. (2023).

Fig. 2 shows an exemplary trajectory of the hybrid model found, illustrating a high level of agreement between the first-principle model and the hybrid model.

Global sensitivity analysis (Dixit and Rackauckas, 2022) of the embedded neural network revealed high relevance of the input ϕ, with the other inputs being negligible, as shown in Fig. 3. This is expected due to the structure of the mechanistic model. Minor dependence on other state variables is mainly caused by noise. Due to this, we omit the neural network's dependency on the states other than ϕ and use this smaller network for all control approaches in the following.

2.4. Multistage reactor

As illustrated in Fig. 1 we consider a flow sheet with 3 well mixed diabatic reactors. They will be denoted in the following by the subscript $r \in [1,2,3]$. It is assumed that all three reactors have equal volume with equal amount of catalyst according to

$$\mathrm{V}_r = \frac{\mathrm{V_{tot}}}{3}, \tag{25}$$

$$m_{\mathrm{cat},r} = \frac{\mathrm{m_{cat,tot}}}{3}. \tag{26}$$

Table 2
Parameter values for reaction kinetics model (Seidel et al., 2021).

Parameter	Value	Parameter	Value	Parameter	Value	Unit
$\alpha_{1,1}$	13.814	$\alpha_{1,2}$	15.0921	$\alpha_{1,3}$	1.2777	–
$\alpha_{2,1}$	3784.4	$\alpha_{2,2}$	1581.7	$\alpha_{2,3}$	−2.167	–
$\alpha_{3,1}$	−9.2833	$\alpha_{3,2}$	−8.7639	$\alpha_{3,3}$	0.5194	–
$\alpha_{4,1}$	$3.1475\cdot10^{-3}$	$\alpha_{4,2}$	$2.1105\cdot10^{-3}$	$\alpha_{4,3}$	$-1.037\cdot10^{-3}$	–
$\alpha_{5,1}$	$-4.2613\cdot10^{-7}$	$\alpha_{5,2}$	$-1.9303\cdot10^{-7}$	$\alpha_{5,3}$	$2.331\cdot10^{-7}$	–
A_{CO}	−5.001	A_{CO_2}	−3.145	A_{WGS}	−4.4526	mol bar^{-3} kg$_{cat}^{-1}$ s^{-1}
B_{CO}	26.455	B_{CO_2}	1.5308	B_{WGS}	15.615	–
$\beta_{H_2}^{(red)}$	1.1064	–	–	–	–	bar$^{-0.5}$
$\beta_{CO}^{(oxi)}$	0.14969	$\beta_{CO_2}^{(het)}$	0.062881	–	–	bar^{-1}
ΔG_1	335.7	ΔG_2	21 841.5	–	–	J mol^{-1}
k_1^+	$79.174\cdot10^{-4}$	k_2^+	$0.188\cdot10^{-4}$	–	–	s^{-1}
ϕ_{max}	0.9	–	–	–	–	–

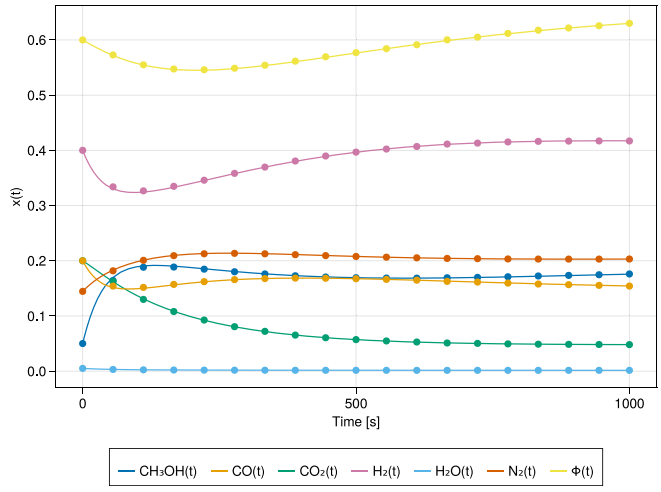

Fig. 2. Example trajectory comparing the first-principle (solid) and the hybrid model (dotted).

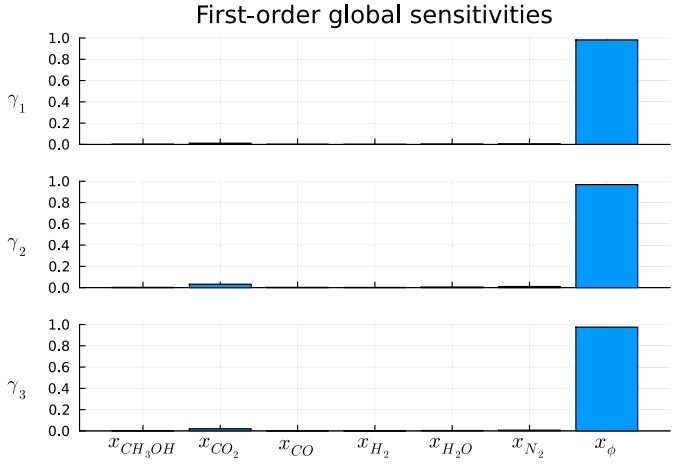

Fig. 3. Global sensitivities of the found neural network with respect to its inputs. The sensitivity analysis reveals a strong dependency on the state ϕ, which is called x_ϕ in this figure, while the other inputs are less influential on the output of the neural net.

$\dot{n}_{\text{in,tot}}$ in Fig. 1 is the total inlet flow rate it consists of a fluctuating hydrogen supply $\xi\cdot\dot{n}_{\text{H}_2,\text{in,tot}}$ and a mixed CO, CO_2 carbon supply $\dot{n}_{\text{C,in,tot}}$, with ψ_C being the molar ratio of CO_2 to CO in the feed

$$\dot{n}_{\text{in,tot}} = \xi\cdot\dot{n}_{\text{H}_2,\text{in,tot}} + \dot{n}_{\text{C,in,tot}}, \tag{27}$$

$$y_{\text{H}_2,in,tot} = \frac{\xi\cdot\dot{n}_{\text{H}_2,\text{in,tot}}}{\dot{n}_{\text{in,tot}}}, \tag{28}$$

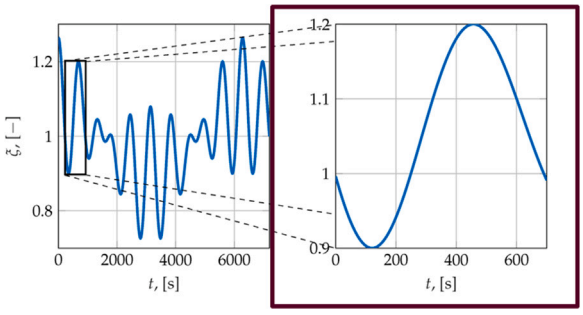

Fig. 4. Hydrogen supply disturbance scenario taken from Keßler and Kienle (2023). Left: Domain relevant for robust steady states design in Keßler and Kienle (2023). Right: Specific scenario considered in this paper. $\dot{n}_{H_2,tot,in} = \xi\dot{n}_{H_2,ref}$.

$$y_{\text{CO}_2,\text{in,tot}} = \frac{\dot{n}_{\text{C,in,tot}}\cdot\psi_{\text{C}}}{\dot{n}_{\text{in,tot}}}, \tag{29}$$

$$y_{\text{CO},in,tot} = \frac{\dot{n}_{\text{C,in,tot}}\cdot\left(1-\psi_{\text{C}}\right)}{\dot{n}_{\text{in,tot}}}. \tag{30}$$

The fresh feed is divided by split-ratios, κ_r, to the three reactors with

$$\dot{n}_{\text{in},1} = \kappa_1\cdot\dot{n}_{\text{in,tot}}, \tag{31}$$

$$\dot{n}_{\text{in},\bar{r}} = \kappa_{\bar{r}}\cdot\dot{n}_{\text{in,tot}} + \dot{n}_{\text{out},\bar{r}-1}, \quad \bar{r}\in[2,3], \tag{32}$$

$$\sum_r \kappa_r = 1. \tag{33}$$

The inlet compositions and temperatures for reactors 2 and 3 are calculated accordingly with

$$\boldsymbol{y}_{\text{in},\bar{r}} = \frac{\boldsymbol{y}_{\bar{r}-1}\cdot\dot{n}_{\text{out},\bar{r}-1} + \kappa_{\bar{r}}\cdot\dot{n}_{\text{in,tot}}\cdot\boldsymbol{y}_{\text{in,tot}}}{\dot{n}_{\text{out},\bar{r}-1} + \kappa_{\bar{r}}\cdot\dot{n}_{\text{in,tot}}}, \tag{34}$$

$$T_{\text{in},\bar{r}} = \frac{T_{\bar{r}-1}\cdot\dot{n}_{\text{out},\bar{r}-1} + \kappa_{\bar{r}}\cdot\dot{n}_{\text{in,tot}}\cdot T_{\text{in,tot}}}{\dot{n}_{\text{out},\bar{r}-1} + \kappa_{\bar{r}}\cdot\dot{n}_{\text{in,tot}}}, \tag{35}$$

where $T_{\text{in,tot}}$ is the temperature of the inlet into the system.

Parameters $\dot{n}_{\text{C,in,tot}}, \xi\cdot\dot{n}_{\text{H}_2,\text{in,tot}}, \psi_C, T_{\text{in,tot}}$ and cooling temperatures of the reactors have been taken from the robust design in Keßler and Kienle (2023).

3. Control concept

In this paper a two degrees of freedom (2 DOF) control strategy is proposed to compensate unavoidable fluctuations in the feed supply. Main source of disturbances is the hydrogen feed which is produced by electrolysis with renewable energy (e.g. wind energy in our scenario). It is assumed that fluctuations of the hydrogen supply can be well predicted over a time horizon of a few hours. A representative disturbance scenario considered in this paper is shown in Fig. 4. It resembles a typical wind scenario. For the details the reader is referred to Keßler and Kienle (2023).

Table 3
Variables and respective bounds. Variables below the mid rule are degrees of freedom.

Variable	Domain	Unit
$\boldsymbol{T}$	[400, 600]	K
$\dot{\boldsymbol{V}}_{\text{out}}$	$[1\cdot10^{-4}, 5\cdot10^{-1}]$	$m^3\ s^{-1}$
$\boldsymbol{T}_{\text{c}}^{*}$	[450, 550]	K
$\boldsymbol{T}_{\text{c,s}}^{*}$	[450, 550]	K
$\boldsymbol{\kappa}^{*}$	[0, 1]	–
$\boldsymbol{\kappa}_{s}^{*}$	[0, 1]	–
s_1^{*}	[0, 0.6]	–
s_2^{*}	[0, 100]	–

To counteract this disturbance, feedforward control action is calculated with dynamic optimization as described in Keßler and Kienle (2023). However, in contrast to Keßler and Kienle (2023) we use the hybrid model introduced in the previous section instead of the mechanistic model for dynamic optimization in the feed forward part. Manipulated variables of the feed forward controller are the feed splits and the shell temperatures of the different reactors. The corresponding dynamic optimization problem is defined as:

$$
\begin{aligned}
\max_{\boldsymbol{x}} \quad & J = \int STY\,(\boldsymbol{x},\xi)^2\,/t_{\text{end}}^2 - \mathrm{U}\cdot(s_1+s_2)\,\mathrm{d}t \\
\text{s.t.} \quad & \text{dynamic hybrid model equations,} \\
& \boldsymbol{x}^{\text{lo}} \le \boldsymbol{x} \le \boldsymbol{x}^{\text{up}}, \\
& X_{\text{C}}(\boldsymbol{x},\xi) + s_1 \ge 0.6, \\
& \left(\boldsymbol{T}(\boldsymbol{x},\xi) - \boldsymbol{T}_c\right)^2 \le (30+s_2)^2, \\
& \textstyle\sum_i y_i(\boldsymbol{x},\xi) = 1, \\
& \textstyle\sum_i y_{i,\text{in}} = 1, \\
& \dot{\boldsymbol{T}}_c = \dfrac{-\boldsymbol{T}_c + \boldsymbol{T}_{c,s}}{50}, \\
& \dot{\boldsymbol{\kappa}} = \dfrac{-\boldsymbol{\kappa} + \boldsymbol{\kappa}_s}{20},
\end{aligned}
\tag{OP}
$$

where the objective is the integral over time of STY, the space time yield, which is defined as

$$
STY = \left(\frac{\dot{n}_{out,3}\cdot y_{\text{CH}_3\text{OH},3}}{V_{tot}}\right), \tag{36}
$$

and X_C is the carbon conversion

$$
X_C = \left(\frac{\dot{n}_{out,3}\cdot y_{\text{CH}_3\text{OH},3}}{\dot{n}_{C,in,tot}}\right) \tag{37}
$$

which should be at least 60%. Further, since the hydrogenation reactions are exothermic, a constraint of 30 K between reactor and shell temperatures is introduce to prevent hotspot formation (Fischer and Freund, 2020). $\boldsymbol{s}$ are slack variables, and U = 100 is a penalty constant, both of which have been chosen empirically. The slack variables allow for the violation of the constraints at the expense of a highly reduced cost function, which is therefore avoided as much as possible. Note, that the constraints are not violated in the final results, but the slack variables make it easier for the solver to find proper starting points and, hence, speed up the optimization process. To avoid spontaneous, switching of control variables, which is not feasible in practice, additional first order lag systems were introduced for the feed split and the shell temperatures according to the last two equations in the problem definition above. The variables and their bounds are listed in Table 3.

The optimization problem was implemented in Julia (Bezanson et al., 2017), using the JuMP (Lubin et al., 2023) based package InfiniteOpt (Pulsipher et al., 2021). A forward finite difference approach with 150 discretization points is used to discretize the time domain. The problem is solved using the NLP solver KNITRO (Byrd et al., 2006).

To compensate plant model mismatch (considered in this paper) and additional unforeseen disturbances (not explicitly considered in this paper), feedforward control action is complemented by a feedback

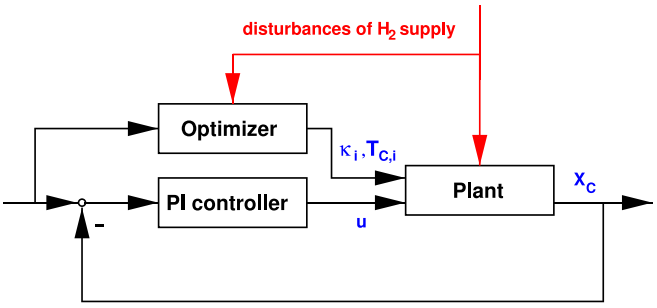

Fig. 5. 2 DOF control scheme proposed in this paper. Feedforward control variables: feed splits - κ_i, cooling temperatures - $T_{C,i}$, feedback control variable: fraction of nominal carbon feed - u, output variable: Carbon conversion - X_c.

controller. In particular, a simple PI controller is used

$$
u = 1 + \mathrm{K_p}\left(e + \frac{1}{\mathrm{T_i}}\int e\,\mathrm{d}t\right) \tag{38}
$$

with parameters $\mathrm{K_p} = 0.6$ and $\mathrm{T_i} = 1$ obtained empirically by the stability margin method (see e.g. Luyben and Luyben (1997)). Controlled variable is the conversion X_C. Manipulated variable is associated with the carbon feed supply, which can be changed by a factor u, which is multiplied with $\dot{n}_{\text{in,C}}$. In the nominal case, with zero control error e, u equals 1. The final control strategy is illustrated in Fig. 5.

4. Results and discussion

In this section the control strategy is implemented and tested step by step by means of the detailed reference model to study also the effect of plant model mismatch. In a first step, feedforward control action is calculated by dynamic optimization with the hybrid model. Results are illustrated in Fig. 6. Manipulated variables are the feed split and the shell temperatures. In the beginning, fresh feed is mainly fed to the first and the third reactor. Feed to the first reactor is increasing with decreasing hydrogen supply in Fig. 4, feed to the third reactor is decreasing with decreasing hydrogen supply, and vice versa as the hydrogen supply is increasing again. As the hydrogen supply is further increasing beyond its initial value, the feed to the first reactor is step by step redirected to the second reactor and back again to the first reactor as the hydrogen supply is dropping in the end again. Shell temperatures are at the lower bound for reduced hydrogen supply in the first phase and increase step by step with increasing hydrogen supply. The lag becomes obvious in the final phase where hydrogen is decreasing again, but the temperatures are staying close to their upper bound. Carbon conversion is most of the time close to the lower bound, with some positive deviations at the beginning and the end.

For validation of the optimization results, control profiles for the feed split and the shell temperatures were simulated with the hybrid model. As illustrated in Fig. 7. Simulated mole fractions of methanol, reactor temperatures and molar outlet flows in Fig. 7 show good agreement with the optimization results in Fig. 6. Minor deviations are observed in view of the carbon conversion in both figures. This is due to the larger integration error of the simpler finite difference method applied for the dynamic optimization compared to the simulation. The dynamic simulation was done with IDA from the SUNDIALS library, which is a more advanced fully implicit BDF method (Hindmarsh et al., 2005).

To demonstrate the effect of plant model mismatch between the detailed mechanistic plant model and the hybrid model used for the dynamic optimization, the optimal control profiles for the feed split and the shell temperatures were next simulated with the reference model. Results are illustrated in Fig. 8. Differences to Fig. 7 become most obvious for the carbon conversion. It turns out that carbon conversion predicted by the detailed model is violating the 60% constraint

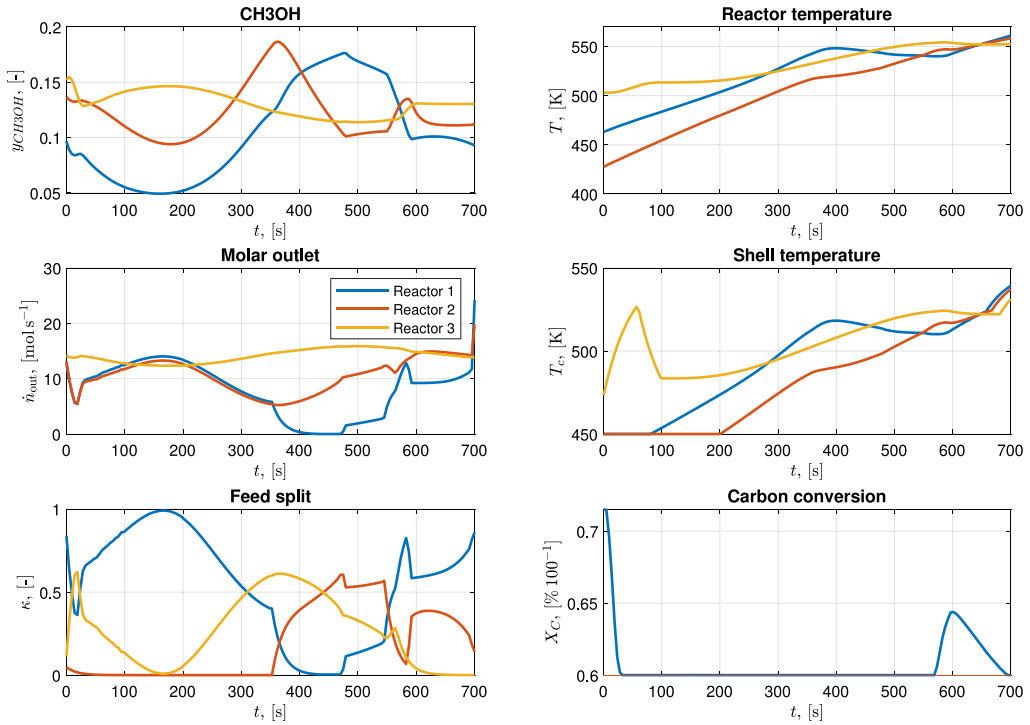

Fig. 6. Optimal control profiles for the feed split and the shell temperatures and corresponding temporal evolution of mole fractions of CH_3OH, reactor temperatures and molar outlets of all three reactors, and total carbon conversion of the multistage reactor. Results obtained by dynamic optimization of the hybrid model.

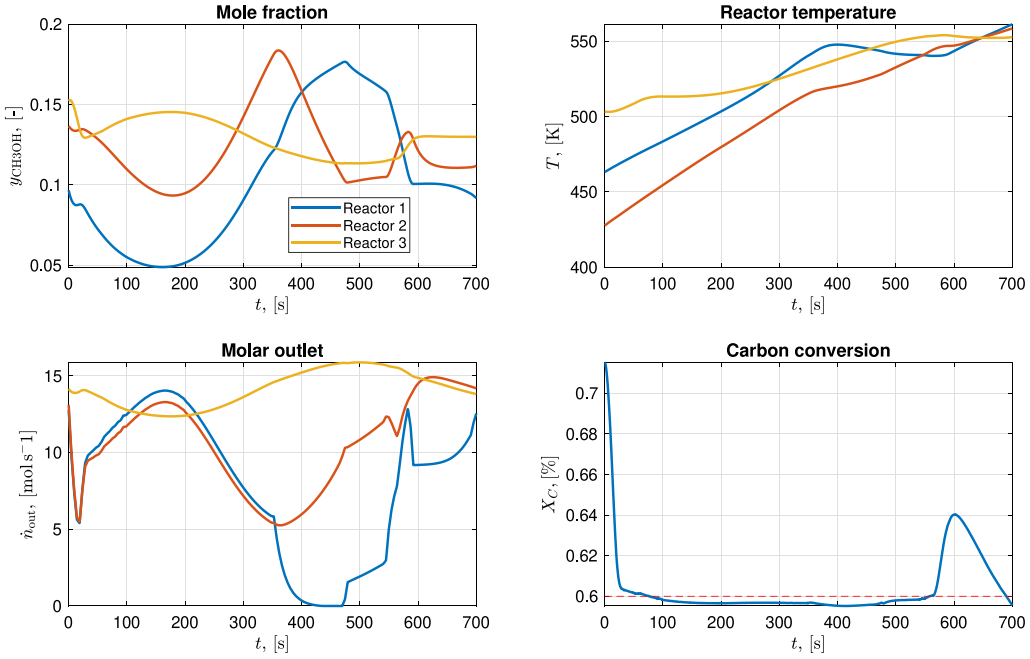

Fig. 7. Temporal evolution of mole fractions of CH_3OH, reactor temperatures and molar outlets of all three reactors, and total carbon conversion of the multistage reactor. Simulation results obtained with hybrid model and optimal control profiles for the feed split and the shell temperatures of the hybrid model from Fig. 6.

nearly over the entire time domain of the considered scenario. This deviation is larger than what was expected in view of Fig. 2. This difference can be explained in the following way. The hybrid model was fitted for isothermal reactor operation, which was applied in Fig. 2. In contrast to this, the control concepts in this chapter are evaluated for nonisothermal (diabatic) reactor operation. Extrapolation of the hybrid model to nonisothermal conditions and to the reactor cascade introduces additional errors.

To handle this plant model mismatch additional feedback control is applied as described in the previous section. Carbon conversion is thereby controlled with an additional handle, which is the fraction of the carbon in the feed. With this combined strategy, the effect of plant model mismatch is efficiently eliminated and carbon conversion can be kept most of the time at its desired setpoint with only very minor deviations as illustrated in Fig. 9. Convergence to the desired setpoint is rapid and relatively smooth with only little overshoot.

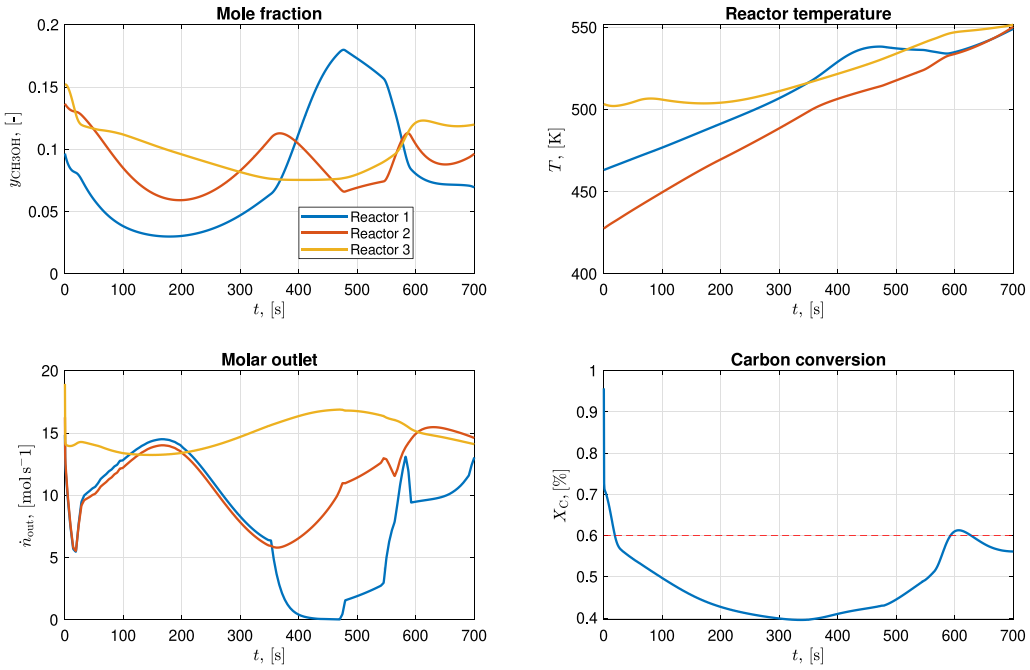

Fig. 8. Temporal evolution of mole fractions of CH_3OH, reactor temperatures and molar outlets of all three reactors, and total carbon conversion of the multistage reactor. Simulation results obtained with the mechanistic reference model and optimal control profiles for the feed split and the shell temperatures of the hybrid model from Fig. 6.

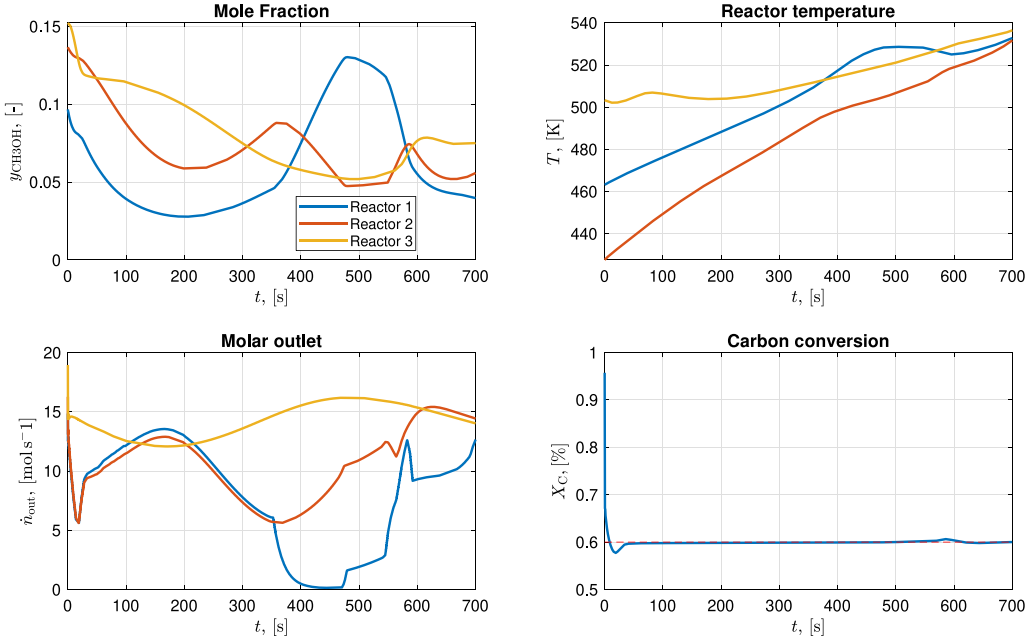

Fig. 9. Temporal evolution of mole fractions of CH_3OH, reactor temperatures and molar outlets of all three reactors, and total carbon conversion of the multistage reactor. Simulation results obtained with the mechanistic reference model and optimal control profiles for the feed split and the shell temperatures of the hybrid from Fig. 6 and additional feedback control according to Eq. (38) to track the desired carbon conversion of 60%.

The required control action for the carbon feed is illustrated in Fig. 10. It is almost proportional to the deviation of the carbon conversion from the 60% line in Fig. 8 with some deviations in particular at later times due to integral action of the feed back controller. In summary, we conclude that the 2 DOF control strategy presented in this paper is very well suited to compensate disturbances and plant model mismatch. Main disturbance compensation is done by the nonlinear feedforward control action, which is calculated by dynamic optimization of the nonlinear hybrid model. Since the hybrid model is in relative good agreement with the reference model as shown in Section 2.3, this strategy works very well and compensation of plant model mismatch by linear feedback control action is, though not negligible, minor compared to the feedforward action and can be handled effectively by the linear feedback controller.

5. Conclusion and outlook

In this paper a new efficient and robust two degrees of freedom control strategy was developed for a multistage power-to-methanol reactor and tested in silico. It was assumed that main disturbances are

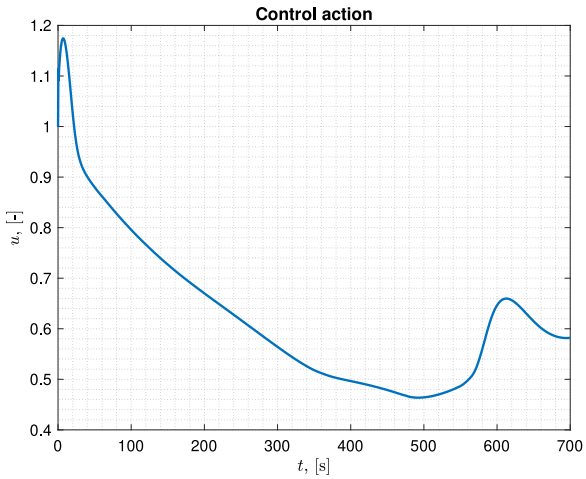

Fig. 10. Control action according to Eq. (38) which is required to track the desired carbon conversion of 60% in Fig. 9.

introduced by the green hydrogen supply due to unavoidable fluctuations of regenerative electrical energy supply for water electrolysis. In this contribution, a scenario with disturbances on a relatively short time horizon of about 10 min, typical for regenerative energy supply from wind turbines, was considered. In view of the time required for hydrogen production and in view of moderate intermediate storage capacities, it was assumed that the disturbance of the hydrogen supply can be well predicted on this time horizon. However, uncertainty of disturbance prediction is increasing with increasing time horizon. Nowadays a good prediction of energy supply from wind turbines over a few hours seems to be possible. For longer time horizons, the present control strategy could be embedded in a receding horizon strategy, where feedforward control action is re-calculated from time to time to include updates of the predicted disturbances. Further, the receding horizon strategy could also be used for updating the hybrid model with available new measurement information from the process.

The proposed control strategy was based on a hybrid model, which combines physico-chemical modeling from first principles with a data driven neural network to predict the influence of dynamic changes of the catalyst on the reaction rates, which can be hard to model from first principles. This hybrid model combines good predictability due to the inclusion of physico-chemical a priori knowledge with high efficiency due to the data driven approach. The approach was well motivated by our previous work on mathematical modeling of the methanol kinetics (Seidel et al., 2018, 2020). However, alternative hybrid model structures are possible by replacing the reaction kinetics step-by-step by data driven models and thereby relaxing more and more the effort for kinetic modeling. This would also be interesting for new reaction systems, where not yet so much a priori knowledge is available like for the methanol synthesis. Therefore an interesting question for our future work is also to study how the performance of the proposed control scheme depends on the specific hybrid model structure. Again, methanol synthesis could be a suitable benchmark problem for this.

Finally, it is clear that the proposed control strategy cannot handle all possible disturbance scenarios. For example, it would not work if there is very little or even no wind available at all. For such cases, additional measures are required like buffer tanks for example. To find an optimal trade off between different strategies is also an interesting topic, which is, however, beyond the scope of this paper.

CRediT authorship contribution statement

Tobias Keßler: Writing – review & editing, Visualization, Software, Methodology, Conceptualization. **Christoph Plate:** Writing – review & editing, Software, Methodology. **Jessica Behrens:** Writing – review & editing, Methodology. **Carl J. Martensen:** Writing – review & editing, Software, Methodology. **Johannes Leipold:** Writing – review & editing, Visualization, Methodology. **Lothar Kaps:** Writing – review & editing, Methodology. **Andreas Seidel-Morgenstern:** Writing – review & editing, Funding acquisition. **Sebastian Sager:** Writing – review & editing, Funding acquisition. **Achim Kienle:** Writing – review & editing, Writing – original draft, Supervision, Methodology, Funding acquisition, Conceptualization.

Declaration of competing interest

The authors declare that they have no known competing financial interests or personal relationships that could have appeared to influence the work reported in this paper.

Acknowledgments

The financial support of the German Science Foundation DFG within in the Priority Program ‘Machine learning in Chemical Engineering’ under grants KI 471/9-1, SA 2016/3-1, SE 586/25-1 is greatly acknowledged.

Data availability

Data will be made available on request.

References

Abrol, S., Hilton, C.M., 2012. Modeling, simulation and advanced control of methanol production from variable synthesis gas feed. Comput. Chem. Eng. 40, 117–131.
Allman, A., Palys, M., Daoutidis, P., 2019. Scheduling-informed optimal design of systems with time-varying operation: A wind-powered ammonia case study. AIChE J. 65, e16434.
Asinger, F., 1986. Methanol - Chemie Und Energierohstoff. Springer.
Beek, M.V., Sadlowski, M., 2020. Transient optimization of coproduction systems for steel and value-added chemicals. Chem. Ing. Tech. 92, 1431–1443.
Bezanson, J., Edelman, A., Karpinski, S., Shah, V.B., 2017. Julia: A fresh approach to numerical computing. SIAM Rev. 59, 65–98. http://dx.doi.org/10.1137/141000671, URL: https://epubs.siam.org/doi/10.1137/141000671.
Bos, M., Kersten, S., Brilman, D., 2020. Wind power to methanol: Renewable methanol production using electricity, electrolysis of water and co2 air capture. Appl. Energy 264, 114672. http://dx.doi.org/10.1016/j.apenergy.2020.114672.
Burre, J., Bongartz, D., Brée, L., Roh, K., Mitsos, A., 2020. Power-to-x: Between electricity storage, e-production, and demand side management. Chem. Ing. Tech. 92, 74–84.
Bussche, K., Froment, G., 1996. A steady-state kinetic model for methanol synthesis and the water gas shift reaction on a commercial Cu/ZnO/Al_2O_3 catalyst. J. Catal. 161, 1–10. http://dx.doi.org/10.1006/jcat.1996.0156.
Byrd, R.H., Nocedal, J., Waltz, R.A., 2006. Knitro: An Integrated Package for Nonlinear Optimization. Springer US, Boston, MA, pp. 35–59. http://dx.doi.org/10.1007/0-387-30065-1_4.
Dixit, V., Rackauckas, C., 2022. Globalsensitivity.jl: Performant and parallel global sensitivity analysis with julia. J. Open Source Softw. 7, 4561. http://dx.doi.org/10.21105/joss.04561.
Fiedler, E., Grossmann, G., Kersebohm, D.B., Weiss, G., Witte, C., 2000. Methanol - Chemie Und Energierohstoff. Wiley-VCH.
Fischer, K.L., Freund, H., 2020. Intensification of load flexible fixed bed reactors by optimal design of staged reactor setups. Chem. Eng. Process. 159, 108183.
Graaf, G., Sijtsema, P., Stamhuis, E., Joosten, G., 1986. Chemical equilibria in methanol synthesis. Chem. Eng. Sci. 41, 2883–2890. http://dx.doi.org/10.1016/0009-2509(86)80019-7.
Graaf, G., Stamhuis, E., Beenackers, A., 1988. Kinetics of low-pressure methanol synthesis. Chem. Eng. Sci. 43, 3185–3195. http://dx.doi.org/10.1016/0009-2509(88)85127-3.
Hindmarsh, A.C., Brown, P.N., Grant, K.E., Lee, S.L., Serban, R., Shumaker, D.E., Woodward, C.S., 2005. SUNDIALS: Suite of nonlinear and differential/algebraic equation solvers. ACM Trans. Math. Softw. 31, 363–396. http://dx.doi.org/10.1145/1089014.1089020.
Keßler, T., Kienle, A., 2023. Robust design and operation of a multistage reactor for methanol synthesis from renewable resources. Processes 11 (10), 2928.
Lubin, M., Dowson, O., Garcia, J.D., Huchette, J., Legat, B., Vielma, J.P., 2023. Jump 1.0: Recent improvements to a modeling language for mathematical optimization. Math. Prog. Comp. 15, 581–589. http://dx.doi.org/10.1007/s12532-023-00239-3.

Luyben, W.L., Luyben, M.L., 1997. Essentials of Process Control. Mc Graw Hill.

Martensen, C.J., Plate, C., Keßler, T., Kunde, C., Kaps, L., Kienle, A., Seidel-Morgenstern, A., Sager, S., 2023. Towards machine learning for Power2X processes. Comput. Aided Chem. Eng. 52, 561–568. http://dx.doi.org/10.1016/B978-0-443-15274-0.50089-5.

Martin, M., 2016. Methodology for solar and wind energy chemical storage facilities design under uncertainty: Methanol production from co2 and hydrogen. Comput. Chem. Eng. 92, 43–54.

Mucci, S., Mitsos, A., Bongartz, D., 2023. Cost-optimal power-to-methanol: flexible operation or intermediate storage? J. Energy Storage 72, 108614.

Nestler, F., Krüger, M., Full, J., Hadrich, M.J., White, R.J., Schaadt, A., 2018. Methanol synthesis – industrial challenges within a changing raw material landscape. Chem. Ing. Tech. 90, 1409–1418. http://dx.doi.org/10.1002/cite.201800026.

Nikolić, D., Seidel, C., Felischak, M., Milicić, T., Kienle, A., Seidel-Morgenstern, A., Petkovska, M., 2022. Forced periodic operations of a chemical reactor for methanol synthesis - The search for the best scenario based on the nonlinear frequency response method. Part I single input modulations. Chem. Eng. Sci. 248 (Part A), 117134.

Pulsipher, J.L., Zhang, W., Hongisto, T.J., Zavala, V.M., 2021. A unifying modeling abstraction for infinite-dimensional optimization. Comput. Chem. Eng. http://dx.doi.org/10.1016/j.compchemeng.2021.107567.

Robinson, P.J., Luyben, W.L., 2011. Plantwide control of a hybrid integrated gasification combined cycle/methanol plant. Ind. Eng. Chem. Res. 50, 4579–4594.

Schlögel, R., 2015. The revolution continues: Energiewende 2.0. Angew. Chem. Int. Ed. 54, 4436–4439.

Seidel, C., Jörke, A., Vollbrecht, B., Seidel-Morgenstern, A., Kienle, A., 2018. Kinetic modelling of methanol synthesis from renewable resources. Chem. Eng. Sci. 175, 130–138.

Seidel, C., Jörke, A., Vollbrecht, B., Seidel-Morgenstern, A., Kienle, A., 2020. Corrigendum to 'Kinetic modeling of methanol synthesis from renewable resources' (Chem. Eng. Sci. 175 (2018) 130-138). Chem. Eng. Sci. 223, 115724.

Seidel, C., Nikolić, D., Felischak, M., Petkovska, M., Seidel-Morgenstern, A., Kienle, A., 2021. Optimization of methanol synthesis under forced periodic operation. Processes 9 (5), 872.

Skrzipek, J., Solczynski, J., Ledakowicz, S., 1994. Methanol Synthesis: Science and Engineering. Polish Scientific Publishers.

Theuerl, S., Herrmann, C., Heiermann, M., Grundmann, P., Landwehr, N., Kreidenweis, U., Kreidenweis, U., Prochnow, A., 2019. The future agricultural biogas plant in germany: A vision. Energies http://dx.doi.org/10.3390/en12030396.

Vita, A., Vita, A., Italiano, C., Previtali, D., Previtali, D., Fabiano, C., Palella, A., Palella, A., Freni, F., Bozzano, G., Pino, L., Manenti, F., 2018. Methanol synthesis from biogas: A thermodynamic analysis. Renew. Energy http://dx.doi.org/10.1016/j.renene.2017.11.029.

Vollbrecht, B., 2007. Zur Kinetik der Methanolsynthese an einem technischen $Cu/ZnO/Al_2O_3$-Katalysator (Ph.D. thesis). Otto-von-Guericke-Universität.